

## 6398 **Optical Elements and Keywords, Complements**

6399 **Abstract** This chapter is not a review of the 60+ optical elements of zgoubi's  
6400 library. They are described in the Users' Guide. One aim here is, regarding some of  
6401 them, to briefly recall some aspects which may not be found in the Users' Guide and  
6402 yet addressed, or referred to, in the theoretical reminder sections and in the exercises.  
6403 This chapter is not a review of the 40+ monitoring and command keywords available  
6404 in zgoubi, either. However it reviews some of the methods used, by keywords such  
6405 as MATRIX (computation of transport coefficients from sets of rays), FAISCEAU  
6406 (which produces beam emittance parameters), and others. This chapter in addition  
6407 recalls the basics of transport and beam matrix methods, in particular it provides the  
6408 first order transport matrix of several of the optical elements used in the exercises, in  
6409 view essentially of comparisons with transport coefficients drawn from raytracing,  
6410 in simulation exercises.

### 6411 **13.1 Introduction**

6412 Optical elements are the basic bricks of charged particle beam lines and accelerators.  
6413 An optical element sequence is aimed at guiding the beam from one location to  
6414 another while maintaining it confined in the vicinity of a reference optical axis.  
6415 Zgoubi library offers of collection of about 100 keywords, amongst which about  
6416 60 are optical elements, the others being commands (to trigger spin tracking, trigger  
6417 synchrotron radiation, print out particle coordinates, compute beam parameters,  
6418 etc.). This library has built over half a century, so it allows simulating most of  
6419 the optical elements met in real life accelerator facilities. Quite often, elements  
6420 available provide different ways to model a particular optical component. A bending  
6421 magnet for instance can be simulated using AIMANT, or BEND, CYCLOTRON,  
6422 DIPOLE[S][-M], FFAG, FFAG-SPI, MULTIPOL, QUADISEX, or a field map and  
6423 TOSCA, CARTEMES or POLARMES to handle it. These various keywords have  
6424 their respective subtleties, though, more on this can be found in the "Optical Elements  
6425 Versus Keywords" Section of the guide [1, page 227], which tells "Which optical

6426 component can be simulated. Which keyword(s) can be used for that purpose”. For  
 6427 a complete inventory of optical elements, refer to the “Glossary of Keywords” found  
 6428 at the beginning of PART A [1, page 9] or PART B of the Users’ Guide [1, page 227].

6429 Optical elements in *zgoubi* are actually field models, or field modeling methods  
 6430 such as reading and handling field maps. Their role is to provide the numerical  
 6431 integrator with the necessary field vector(s) to push a particle further, and possibly  
 6432 its spin, along a trajectory. The following sections introduce the analytical field  
 6433 models which the simulation exercises resort to.

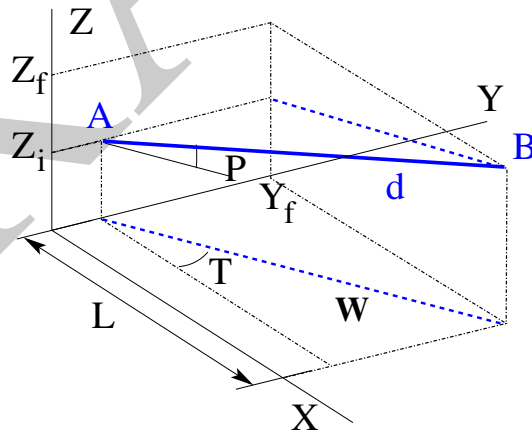
6434 *Zgoubi*’s coordinate nomenclature, as well as the Cartesian or cylindrical refer-  
 6435 ence frames used in the optical elements and field maps, have been introduced in  
 6436 Sect. 1.2 and Fig. 1.5.

### 6437 13.2 Drift Space

6438 This is the DRIFT, or ESL (for the French “ESpace Libre”) optical element, through  
 6439 which a particle moves on a straight line. From the geometry and notations in  
 6440 Fig. 13.1, with  $L$  the length of the drift, coordinate transport satisfies

$$\begin{cases} X_f - X_i = L \\ Y_f - Y_i = L \tan T \\ Z_f - Z_i = L \tan P / \cos T \\ \text{path length } d = L / (\cos T \cos P) \end{cases} \quad (13.7)$$

**Fig. 13.1** An  $L$ -long drift in *zgoubi* ( $O;X,Y,Z$ ) frame, with origin at the start of the drift. A particle flies from  $A(Y_i, Z_i)$  to  $B(Y_f, Z_f)$ , at an angle  $P$  to the  $(X, Y)$  plane. Projection  $W$  of its straight path in  $(X, Y)$  plane is at an angle  $T$  to the  $X$  axis



6441 *Linear approach*

6442 Coordinate transport from initial to final position in the linear approximation is  
 6443 written (with  $z$  standing indifferently for  $x$  or  $y$ , subscripts  $i$  for initial and  $f$  for final  
 coordinates) (Fig. 13.2)

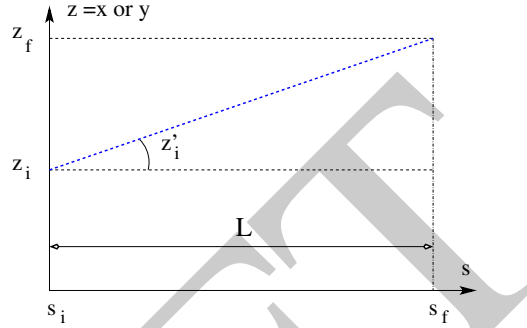


**Fig. 13.2** A drift section with length  $L = s_f - s_i$ , and projection of a straight trajectory in the  $(s, z)$  plane, at an angle  $z'$  (standing for  $x'$  or  $y'$ ) to the  $s$  axis

6444

$$\begin{cases} z_f = z_i + L z'_i \\ z'_f = z'_i \\ \delta l_f - \delta l_i = \beta c \delta t = \frac{L}{\gamma^2} \frac{\delta p}{p} \\ \delta p_f / p = \delta p_i / p \end{cases} \quad \text{or, } T_{\text{drift}} = \begin{pmatrix} 1 & L & 0 & 0 & 0 & 0 \\ 0 & 1 & 0 & 0 & 0 & 0 \\ 0 & 0 & 1 & L & 0 & 0 \\ 0 & 0 & 0 & 1 & 0 & 0 \\ 0 & 0 & 0 & 0 & 1 & \frac{L}{\gamma^2} \\ 0 & 0 & 0 & 0 & 0 & 1 \end{pmatrix} \quad (13.8)$$

6445 where  $\beta c$  is the particle velocity,  $p = \gamma m \beta c$  its momentum,  $\gamma$  is the Lorentz rela-  
 6446 tivistic factor.

6447 **13.3 Guiding**

6448 Beam guiding is in general assured using dipole magnets to provide a uniform field,  
 6449 normal to the bend plane. Gradient dipoles combine guiding and focusing in a single  
 6450 magnet, this is the case in cyclotrons, this is also the case in some synchrotrons,  
 6451 for instance the BNL AGS [2], the CERN PS [3]. By principle, FFAG dipoles have  
 6452 pole faces shaped to provide a highly non-linear dipole field,  $B \propto r^k$  (Sect. 10).  
 6453 Dipole magnets sometimes include a sextupole component for the compensation of  
 6454 chromatic aberrations [4]. Non-linear optical effects may be introduced by shaping  
 6455 entrance and or exit EFBs, a parabola for instance for  $x^2$  field integral dependence,  
 6456 a cubic curve for  $x^3$  dependence (see Chap. 13).

6457 Low energy beam guiding also uses electrostatic deflectors, shaped to provide a  
 6458 field normal to the trajectory arc, and focusing properties. Plane condensers may be

6459 used for beam guiding as well. They are also used at higher energies for some special  
6460 functions, such as pretzel orbit separation, extraction septa, etc.

6461 Guiding optical elements are dispersive systems: trajectory deflection has a first  
6462 order dependence on particle momentum.

### 6463 13.3.1 Dipole Magnet, Curved

6464 This is the DIPOLE element (an evolution of the 1972's AIMANT [1]) or variants:  
6465 DIPOLES, DIPOLE-M. Lines of constant field are isocentric circle arcs. The magnet  
6466 reference curve is a particular arc, at a reference radius  $r_0$ . The field in the median  
6467 plane can be written

$$B_Z(r, \theta) = \mathcal{G}(r, \theta) B_0 \left( 1 + N \frac{r - r_0}{r_0} + N' \left( \frac{r - r_0}{r_0} \right)^2 + N'' \left( \frac{r - r_0}{r_0} \right)^3 + \dots \right) \quad (13.9)$$

6468  $N^{(n)} = d^n N / dY^n$  are the field index and derivatives.  $\mathcal{G}(X)$  describes the longitudinal  
6469 shape of the field, from a plateau value in the body to zero away from the magnet  
6470 (Fig. 13.3). It can be written under the form

$$\mathcal{G}(X) = G_0 F(d(X)) \quad \text{with} \quad G_0 = \frac{B_0}{r_0^{n-1}} \quad (13.10)$$

6471 where  $B_0$  is the field at pole tip at  $r_0$ , and  $F(d)$  a convenient model for the field  
6472 fall-off, *e.g.* (the Enge model, Sect. 13.3.3),

$$F(d) = \frac{1}{1 + \exp[P(d)]}, \quad P(d) = C_0 + C_1 \left( \frac{d}{g} \right) + C_2 \left( \frac{d}{g} \right)^2 + C_3 \left( \frac{d}{g} \right)^3 + \dots \quad (13.11)$$

6473 with  $d$  (an  $X$ -dependent quantity) the distance from  $(X, Y, Z)$  location to the magnet  
6474 EFB,  $g$  the characteristic extent of the field fall-off.

#### 6475 *Linear approach*

6476 In the linear approach the equations of motion of a particle in a dipole magnet, in  
6477 the Serret-Frénet (or “moving”) frame, take the simplified form (a linearization of  
6478 Lorentz force equation)

$$x'' + K_x x = \frac{1}{\rho} \frac{\delta p}{p}, \quad y'' + K_y y = 0 \quad (13.12)$$

where  $K_{x,y}$  constants characterize the magnetic field responsible for the transverse  
acceleration ( $\mathbf{F} = q\mathbf{v} \times \mathbf{B}$ , the acceleration is normal to the velocity vector). In the  
case of a dipole magnet

$$K_x = \frac{1-n}{\rho^2}, \quad K_y = \frac{n}{\rho^2}, \quad \text{with } n = \frac{\rho}{B_y} \frac{\partial B_y}{\partial x} \Big|_{y=0} \text{ the radial field index}$$

6479  $\rho$  the curvature radius, and  $B_y = B_y(y = y_0)$  (this assumes that the magnetic field  
6480  $\mathbf{B}$  features mid-plane anti-symmetry [1, Eq. 1.3.2], which results in  $\mathbf{B}|_{y=0} = \mathbf{B}_y$ ,  
6481  $B_x(y = 0) = 0$  and  $B_z(y = 0) = 0$ ).

The Eq. 13.12 is equivalently formulated as

$$\mathbf{R}(s_2) = T(s_2 \leftarrow s_1) \mathbf{R}(s_1)$$

6482 with  $\mathbf{R}(s_1)$  and  $R(s_2)$  two successive positions of the particle, and  $T(s_2 \leftarrow s_1)$  the  
6483 transfer (or “transport”) matrix from  $R(s_1)$  to  $R(s_2)$ .

6484 The first order transport matrix of a sector dipole with curvature radius  $\rho$ , deflection  
6485  $\alpha$  and index  $n$ , in the hard-edge model, writes

$$T_{\text{bend}} = \begin{pmatrix} C_x & S_x & 0 & 0 & 0 & \frac{r_x^2}{\rho} (1 - C_x) \\ C'_x & S'_x & 0 & 0 & 0 & \frac{1}{\rho} S_x \\ 0 & 0 & C_y & S_y & 0 & 0 \\ 0 & 0 & C'_y & S'_y & 0 & 0 \\ \frac{1}{\rho} S_x & \frac{r_x^2}{\rho} (1 - C_x) & 0 & 0 & 1 & \frac{r_x^3}{\rho^2} (\rho\alpha - S_x) \\ 0 & 0 & 0 & 0 & 0 & 1 \end{pmatrix} \quad \text{with} \quad \begin{cases} C = \cos \frac{\rho\alpha}{r} \\ C' = \frac{dC}{ds} = \frac{1}{\rho} \frac{dC}{d\alpha} = -\frac{S}{r^2} \\ S = r \sin \frac{\rho\alpha}{r} \\ S' = \frac{dS}{ds} = \frac{1}{\rho} \frac{dS}{d\alpha} = C \\ (*)_x : r = \rho/\sqrt{1-n} \\ (*)_y : r = \rho/\sqrt{n} \end{cases} \quad (13.13)$$

6486 or, explicitly,

$$T_{\text{bend}} = \begin{pmatrix} \cos \sqrt{1-n}\alpha & \frac{\rho}{\sqrt{1-n}} \sin \sqrt{1-n}\alpha & 0 & 0 & 0 & \frac{\rho}{1-n} (1 - \cos \sqrt{1-n}\alpha) \\ -\frac{\sqrt{1-n}}{\rho} \sin \sqrt{1-n}\alpha & \cos \sqrt{1-n}\alpha & 0 & 0 & 0 & \frac{1}{\sqrt{1-n}} \sin \sqrt{1-n}\alpha \\ 0 & 0 & \cos \sqrt{n}\alpha & \frac{\rho}{\sqrt{n}} \sin \sqrt{n}\alpha & 0 & 0 \\ 0 & 0 & -\frac{\sqrt{n}}{\rho} \sin \sqrt{n}\alpha & \cos \sqrt{n}\alpha & 0 & 0 \\ \frac{1}{\sqrt{1-n}} \sin \sqrt{1-n}\alpha & \frac{\rho}{1-n} (1 - \cos \sqrt{1-n}\alpha) & 0 & 0 & 1 & \frac{\rho}{(1-n)^{3/2}} (\sqrt{1-n}\alpha - \sin \sqrt{1-n}\alpha) \\ 0 & 0 & 0 & 0 & 0 & 1 \end{pmatrix} \quad (13.14)$$

6487 Cancel the index in the previous sector dipole, introduce a wedge angle  $\varepsilon$  at  
6488 entrance and exit EFBs. The first order transport matrix, accounting for the entrance  
6489 and exit EFB wedge focusing (see Sect. 13.4.1), writes

$$T_{\text{bend}} = \begin{pmatrix} \frac{\cos(\alpha-\varepsilon)}{\cos \varepsilon} & \frac{\rho \sin \alpha}{\cos(\alpha-\varepsilon)} & 0 & 0 & 0 & \frac{\rho(1-\cos \alpha)}{\cos \varepsilon} \\ -\frac{\sin(\alpha-2\varepsilon)}{\rho \cos^2 \varepsilon} & \frac{\cos(\alpha-\varepsilon)}{\cos \varepsilon} & 0 & 0 & 0 & \frac{\sin(\alpha-\varepsilon) + \sin \varepsilon}{\cos \varepsilon} \\ 0 & 0 & 1 - \alpha \tan \varepsilon & \rho\alpha & 0 & 0 \\ 0 & 0 & -\frac{\tan \varepsilon}{\rho} (2 - \alpha \tan \varepsilon) & 1 - \alpha \tan \varepsilon & 0 & 0 \\ \sin \alpha & 0 & 0 & 0 & 1 & \rho(\alpha - \sin \alpha) \\ 0 & 0 & 0 & 0 & 0 & 1 \end{pmatrix} \quad (13.15)$$

6490

### 6491 13.3.2 Dipole Magnet, Straight

6492 This is the MULTIPOL element. Lines of constant field are straight lines. An early in-  
6493 stance of a straight dipole magnet is the AGS main dipole (Fig. 9.2), which combines

6494 steering and focusing, and features in addition a noticeable sextupole component [5].  
 6495 The multipole components  $B_n(X, Y, Z)$  [ $n=1$  (dipole), 2 (quadrupole), 3 (sextupole),  
 6496 ...] in the Cartesian frame of the straight dipole derive, by differentiation, from the  
 6497 scalar potential

$$V_n(X, Y, Z) = (n!)^2 \left( \sum_{q=0}^{\infty} (-1)^q \frac{\mathcal{G}^{(2q)}(X)(Y^2 + Z^2)^q}{4^q q!(n+q)!} \right) \left( \sum_{m=0}^n \frac{\sin\left(\frac{m\pi}{2}\right) Y^{n-m} Z^m}{m!(n-m)!} \right) \quad (13.16)$$

6498 where  $\mathcal{G}^{(2q)}(X) = d^{2q}\mathcal{G}(X)/dX^{2q}$ . In the case of pure dipole field for instance

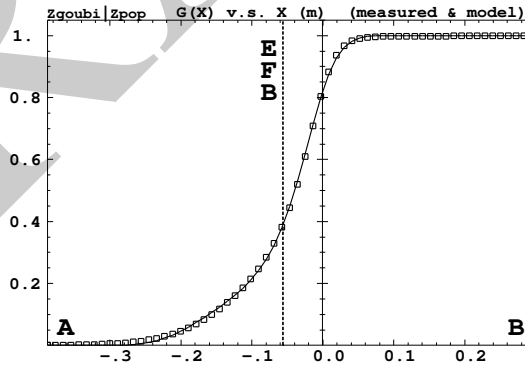
$$V_1(X, Y, Z) = \mathcal{G}(X) Z - \frac{\mathcal{G}''(X)}{8}(Y^2 + Z^2) + \frac{\mathcal{G}^{(4)}(X)}{512}(Y^2 + Z^2) Z \dots \quad (13.17)$$

6499 and

$$\begin{aligned} B_X(X, Y, Z) &= -\frac{\partial V_1}{\partial X} = \mathcal{G}'(X) Z - \frac{\mathcal{G}'''(X)}{8}(Y^2 + Z^2) \dots \\ B_Y(X, Y, Z) &= -\frac{\partial V_1}{\partial Y} = -\frac{\mathcal{G}''(X)}{4} Y + \frac{\mathcal{G}^{(4)}(X)}{256} Y Z \dots \\ B_Z(X, Y, Z) &= -\frac{\partial V_1}{\partial Z} = \mathcal{G}'(X) - \frac{\mathcal{G}''(X)}{4} Z + \frac{3\mathcal{G}^{(4)}(X)}{512} Z^2 \dots \end{aligned} \quad (13.18)$$

6500  $\mathcal{G}(r, \theta)$  is a longitudinal form factor to account for the field fall-offs at the ends of the  
 6501 magnet, modeled using Eq. 13.11, with distance  $d$  to the EFB in the latter, a function  
 6502 of  $r$  and  $\theta$ .

**Fig. 13.3** Longitudinal field form factor (Eq. 13.10 - normalized to one) in BNL AGS main bend, taken along the magnet reference axis. Solid line: from Eq. 13.10 with  $g$  and  $C_i$  values from Eq. 13.21. Squares: measured field data.  $X = 0$  is the origin in the field map frame, the vertical dashed line at  $X_{\text{EFB}} = -5.62$  cm is the location of the EFB.



### 6503 13.3.3 Fringe Field, Modeling, Overlapping

6504 A fringe field model is described here, which is resorted to in several optical elements  
6505 of zgoubi's library.

6506 Field shape at the EFBs of magnetic or electrostatic devices can be simulated  
6507 using a hard-edge model (the field is assumed to change following a Heaviside step).  
6508 When using stepwise ray-tracing techniques however, a smooth change of the field  
6509 can easily be accounted for. An efficient model is Enge's field form factor [6].

$$F(d) = \frac{1}{1 + \exp P(d)} \quad (13.19)$$

$$P(d) = C_0 + C_1 \left(\frac{d}{\lambda}\right) + C_2 \left(\frac{d}{\lambda}\right)^2 + C_3 \left(\frac{d}{\lambda}\right)^3 + C_4 \left(\frac{d}{\lambda}\right)^4 + C_5 \left(\frac{d}{\lambda}\right)^5$$

6510 where  $d$  is the distance to the field boundary and  $\lambda$  is the extent of the fall-off,  
6511 normally commensurate with gap aperture in a dipole, the radius at pole tip in a  
6512 quadrupole, etc.

6513 As an illustration, Fig. 13.3 shows  $F(d)$  as matched to the measured end fields of  
6514 BNL AGS main magnet (Fig. 13.3) [7, 8], using

$$\lambda = \text{gap aperture} \approx 10 \text{ cm} \quad \text{and} \quad (13.20)$$

$$C_0 = 0.45473, C_1 = 2.4406, C_2 = -1.5088, C_3 = 0.7335, C_4 = C_5 = 0$$

6515 These  $C_i$  coefficient values result from an interpolation to measured field data, which  
6516 are also represented in the figure. The location of the EFB results from the following  
6517 constraint, which is part of the matching: the field integral on the down side of the  
6518 fall-off (the region from A to X=0 in Fig. 13.3) is equal to the complement to 1 of  
6519 the field integral on the rising side of the fall-off (X=0 to B region in the figure),  
6520 which writes

$$\int_{X_A}^{X_{\text{EFB}}} F(X) dX = \int_{X_{\text{EFB}}}^{X_B} dX - \int_{X_{\text{EFB}}}^B F(X) dX \Rightarrow X_{\text{EFB}} = X_B - \int_A^B F(X) dX \quad (13.21)$$

6521 A convenient property of this model is that changing the slope of the fall-off (*i.e.*,  
6522 changing  $\lambda$ ) will not affect the location of the EFB.

6523 Inward fringe field extents may overlap when simulating an optical element  
6524 (Fig. 13.4). A way to ensure continuity of the resulting field form factor in such  
6525 case is to use

$$F = F_E + F_S - 1 \quad \text{or} \quad F = F_E * F_S \quad (13.22)$$

6526 where  $F_E$  ( $F_S$ ) is the entrance (exit) form factor and follows Eq. 13.19. Both expres-  
6527 sions can be extended to more than two EFBs (for instance 4, to account for the 4  
6528 faces of a dipole magnet: entrance and exit faces, inner and outer radial boundaries).  
6529 Note that in that case of overlapping field extents, the field integral is affected, lower-

ing with more pronounced overlapping, it is therefore necessary to change the field value ( $B_0$  in Eq. 13.10 for instance) to recover the proper integrated strength.

### Overlapping Fringe Fields

Zgoubi allows a superposition technique to simulate the field in a series of neighboring magnets. The method consists in computing the mid-plane field at any location ( $R, \theta$ ) by adding individual contributions, namely [9]

$$B_Z(r, \theta) = \sum_{i=1, N} B_{Z,i}(r, \theta) = \sum_{i=1, N} B_{Z,0,i} \mathcal{F}_i(r, \theta) \mathcal{R}_i(r)$$

$$\frac{\partial^{k+l} \mathbf{B}_Z(r, \theta)}{\partial \theta^k \partial r^l} = \sum_{i=1, N} \frac{\partial^{k+l} \mathbf{B}_{Z,i}(r, \theta)}{\partial \theta^k \partial r^l} \quad (13.23)$$

with  $\mathcal{F}_i(r, \theta)$  and  $\mathcal{R}_i(r)$  in each individual dipole in the series (Eqs. 10.7, 10.15). Note that, in doing so it is not meant that field superposition would apply in reality (FFAG magnets are closely spaced, cross-talk may occurs), however it appears to allow closely reproducing magnet computation code outcomes.

### Short Optical Elements

In some cases, an optical element in which fringe fields are taken into account (of any kind: dipole, multipole, electrostatic, etc.) may be given small enough a length,  $L$ , that it finds itself in the configuration schemed in Fig. 13.4: the entrance and/or the exit EFB field fall-off extends inward enough that it overlaps with the other EFB's fall-off. In zgoubi notations, this happens if  $L < X_E + X_S$ . As a reminder [1]: in the presence of fringe fields,  $X_E$  (resp.  $X_S$ ) is the stepwise integration extent added upstream (resp. added downstream) of the actual extent  $L$  of the optical element.

In such case, zgoubi computes field and derivatives along the element using a field form factor  $F = F_E \times F_S$ .  $F_E$  (respectively  $F_S$ ) is the value of the Enge model coefficient (Eq. 13.19) at distance  $d_E$  (resp.  $d_S$ ) from the entrance (resp. exit) EFB.

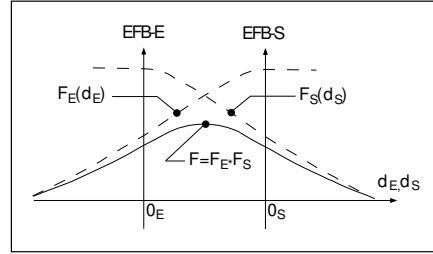
This may have the immediate effect, apparent in Fig. 13.4, that the integrated field is not the expected value  $B \times L$  from the input data  $L$  and  $B$ , and may require adjusting (increasing)  $B$  so to recover the required  $BL$ .

### 13.3.4 Toroidal Condenser

This is the ELCYLDEF element in zgoubi. With proper parameters, it can be used as a spherical, a toroidal or a cylindrical deflector.



**Fig. 13.4** A sketch of overlapping entrance field form factor  $F_E(d_E)$  (at the entrance “EFB-E”) and exit  $F_S(d_S)$  (at the exit “EFB-S”), and resulting form factor  $F = F_E \times F_S$  accounted for in modeling the field within the optical element



Motion along the optical axis, an arc of a circle of radius  $r$  normal to electric field  $\mathbf{E}$ , satisfies

$$Er = v \frac{p}{q} = v(B\rho)$$

6557 with  $p = mv$  the particle momentum,  $q$  its charge and  $(B\rho) = p/q$  the particle  
6558 rigidity.

6559 The first order transport matrix of an electrostatic bend writes

$$T_{\text{condenser}} = \begin{pmatrix} C_x & S_x & 0 & 0 & 0 & \frac{2-\beta^2}{p_x^2} r_0 (1-C_x) \\ C'_x & S'_x & 0 & 0 & 0 & \frac{2-\beta^2}{r_0} S_x \\ 0 & 0 & C_y & S_y & 0 & 0 \\ 0 & 0 & C'_y & S'_y & 0 & 0 \\ -\frac{2-\beta^2}{r_0} S_x & -\frac{2-\beta^2}{p_x^2} r_0 (1-C_x) & 0 & 0 & 1 & r_0 \alpha \left[ \frac{1}{\gamma^2} - \left( \frac{2-\beta^2}{p_x^2} \right)^2 \left( 1 - \frac{S_x}{r_0 \alpha} \right) \right] \\ 0 & 0 & 0 & 0 & 0 & 1 \end{pmatrix} \quad (13.24)$$

with

$$\begin{cases} \alpha = \text{deflection angle} \\ C = \cos p\alpha \\ C' = \frac{dC}{ds} = -\frac{p^2}{r^2} S \\ S = \frac{r}{p} \sin p\alpha \\ S' = \frac{dS}{ds} = C \\ (*)_x : p = p_x = \sqrt{2 - \beta^2 - r_0/R_0} \\ (*)_y : p = p_y = \sqrt{r_0/R_0} \end{cases}$$

6560 **13.4 Focusing**

6561 Particle beams are maintained confined along a reference propagation axis by means  
6562 of focusing techniques and devices. Methods available in zgoubi to simulate those  
6563 are addressed here.

6564 **13.4.1 Wedge Focusing**

6565 Wedge focusing is sketched in Fig. 13.5. A wedge angle  $\varepsilon$  causes a particle at local  
 6566 excursion  $x$  to experience a change  $\int B_y ds = x B_y \tan \varepsilon$  of the field integral compared  
 6567 the field integral through the sector magnet, thus in the linear approximation a change  
 6568 in trajectory angle

$$\Delta x' = \frac{1}{B\rho} \int B_y ds = x \frac{\tan \varepsilon}{\rho_0} \quad (13.25)$$

6569 with  $B\rho$  the particle rigidity and  $\rho_0$  its trajectory curvature radius in the field  $B_0$   
 6570 of the dipole. Vertical focusing results from the non-zero off-mid plane radial field  
 6571 component  $B_x$  in the fringe field region (Fig. 13.7): from (Maxwell's equations)  
 6572  $\frac{\partial}{\partial y} \int B_x ds = \frac{\partial}{\partial x} \int B_y ds$  and Eq. 13.25 the change in trajectory angle comes out to  
 6573 be

$$\Delta y' = \frac{1}{B\rho} \int B_x ds = -y \frac{\tan \varepsilon}{\rho_0} \quad (13.26)$$

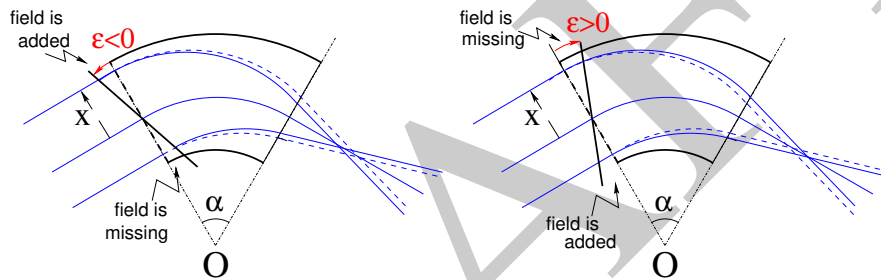


**Fig. 13.5** Left: a focusing wedge ( $\varepsilon < 0$  by convention); opening the sector increases the horizontal focusing. Right: a defocusing wedge ( $\varepsilon > 0$ ); closing the sector decreases the horizontal focusing. The effect is the opposite in the vertical plane, opening/closing the sector decreases/increases the vertical focusing.

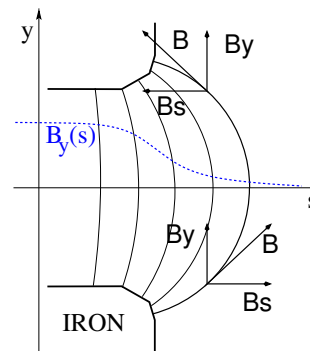


**Fig. 13.6** Field components in the  $B_y(s)$  fringe field region at a dipole EFB

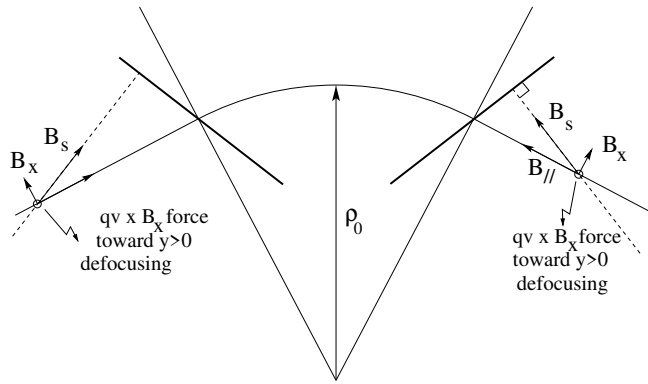


**Fig. 13.7** Field components in the fringe field region at the ends of a dipole ( $y > 0$ , here, referring to Fig. 13.6).  $B_{//}$  is parallel to the particle velocity. This configuration is vertically defocusing: a charged particle traveling off mid-plane is pulled away from the latter under the effect of  $\mathbf{v} \times \mathbf{B}_x$  force component. Inspection of the  $y < 0$  region gives the same result: the charge is pulled away from the median plane

6574 A first order correction  $\psi$  to the vertical kick accounts for the fringe field extent  
6575 (it is a second order effect for the horizontal kick):

$$\Delta y' = -y \frac{\tan(\varepsilon - \psi)}{\rho_0} \quad (13.27)$$

6576 with

$$\psi = I_1 \frac{\lambda}{\rho_0} \frac{1 + \sin^2 \varepsilon}{\cos \varepsilon} \quad \text{with} \quad I_1 = \int_{\text{edge}} \frac{B(s)(B_0 - B(s))}{\lambda B_0^2} ds \quad (13.28)$$

6577  $\lambda$  is the fringe field extent (Sect. 13.3.3),  $I_1$  quantifies the flutter (see Sect. 4.2.1); a  
6578 longer/shorter field fall-off (smaller/greater flutter) decreases/increases the vertical  
6579 focusing.

6580 *Linear approach*

6581 A wedge focusing first order transport matrix writes

$$T_{\text{wedge}} = \begin{pmatrix} 1 & 0 & 0 & 0 & 0 & 0 \\ \frac{\tan \varepsilon}{\rho} & 1 & 0 & 0 & 0 & 0 \\ 0 & 0 & 1 & 0 & 0 & 0 \\ 0 & 0 & -\frac{\tan \varepsilon}{\rho} & 1 & 0 & 0 \\ 0 & 0 & 0 & 0 & 1 & 0 \\ 0 & 0 & 0 & 0 & 0 & 1 \end{pmatrix} \quad (13.29)$$

6582 Substitute  $\varepsilon - \psi$  to  $\varepsilon$  in the  $R_{43}$  coefficient, when accounting for fringe field extent  $\lambda$ .

### 6583 13.4.2 Quadrupole

6584 Most of the time in beam lines and cyclic accelerators, guiding and focusing are  
 6585 separate functions, focusing is assured by quadrupoles, magnetic most frequently,  
 6586 possibly electrostatic at low energy. Quadrupoles are the optical lenses of charged  
 6587 particle beams, they ensure confinement of the beam in the vicinity of the optical  
 6588 axis.

6589 The field in quadrupole lenses results from hyperbolic equipotentials,  $V = axy$ .  
 6590 Pole profiles in quadrupole lenses follow these equipotentials, in a  $2\pi/4$ -symmetrical  
 6591 arrangement for technological simplicity.

#### 6592 13.4.2.1 Magnetic Quadrupole

6593 Magnetic quadrupoles are the optical lenses of high energy beams.

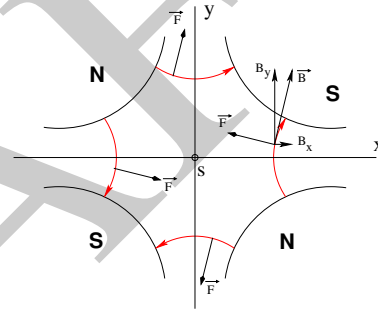
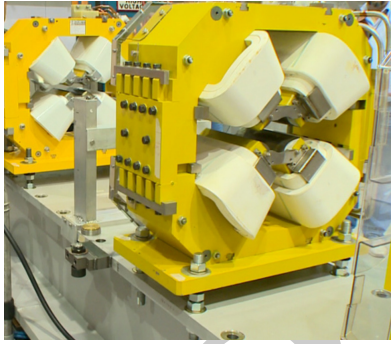


**Fig. 13.8** Left: a quadrupole magnet [11]. Right: field lines and forces (assuming positive charges moving out of the page) over the cross section of an horizontally focusing / vertically defocusing quadrupole

6594 The theoretical field in a quadrupole can be derived from Eq. 13.16 for the scalar  
 6595 potential, with  $n = 2$  which yields

$$V_2(X, Y, Z) = \mathcal{G}(X)YZ - \frac{\mathcal{G}''(X)}{12} (Y^2 + Z^2)YZ + \frac{\mathcal{G}^{(4)}(X)}{384} (Y^2 + Z^2)^2YZ - \dots \quad (13.30)$$

6596 and

$$B_X(X, Y, Z) = -\frac{\partial V_2}{\partial X} = \mathcal{G}'(X)YZ - \frac{\mathcal{G}'''(X)}{12} (Y^2 + Z^2)YZ + \dots \quad (13.31)$$

$$B_Y(X, Y, Z) = -\frac{\partial V_2}{\partial Y} = \mathcal{G}(X)Z - \frac{\mathcal{G}''(X)}{12} (3Y^2 + Z^2)Z + \dots \quad (13.32)$$

$$B_Z(X, Y, Z) = -\frac{\partial V_2}{\partial Z} = \mathcal{G}(X)Y - \frac{\mathcal{G}''(X)}{12} (Y^2 + 3Z^2)Y + \dots \quad (13.33)$$

6597  $\mathcal{G}(X)$  is given by Eq. 13.10 whereas

$$G_0 = \frac{B_0}{r_0} \quad \text{and} \quad K = G_0/B\rho \quad (13.34)$$

6598 define respectively the quadrupole gradient and strength, the latter relative to the  
 6599 rigidity  $B\rho$ . The quadrupole is horizontally focusing and vertically defocusing if  
 6600  $K > 0$ , and the reverse if  $K < 0$ , this is illustrated in Fig. 13.9 which shows a doublet  
 6601 of quadrupoles with focusing strengths of opposite signs.

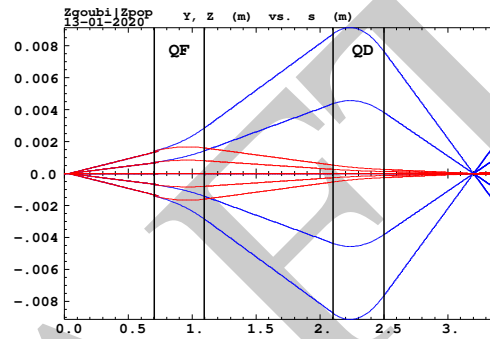


**Fig. 13.9** Horizontal and vertical projections of particle trajectories across a stigmatic quadrupole doublet. The first quadrupole (QF) is horizontally focusing ( $K > 0$ ; thus vertically defocusing), the second one (QD) has the reverse sign ( $K < 0$ )

6602 *Linear approach*

6603 The first order transport matrix of a quadrupole with length  $L$ , gradient  $G$  and  
 6604 strength  $K = G/B\rho$  writes

$$T_{\text{quad}} = \begin{pmatrix} C_x & S_x & 0 & 0 & 0 & 0 \\ C'_x & S'_x & 0 & 0 & 0 & 0 \\ 0 & 0 & C_y & S_y & 0 & 0 \\ 0 & 0 & C'_y & S'_y & 0 & 0 \\ 0 & 0 & 0 & 0 & 1 & \frac{L}{\gamma^2} \\ 0 & 0 & 0 & 0 & 0 & 1 \end{pmatrix} \quad \text{with} \quad \begin{cases} C_x = \cos L\sqrt{K}; C'_x = \frac{dC_x}{dL} = -KS_x \\ S_x = \frac{1}{\sqrt{K}} \sin L\sqrt{K}; S'_x = \frac{dS_x}{dL} = C_x \\ C_y = \cosh L\sqrt{K}; C'_y = \frac{dC_y}{dL} = KS_y \\ S_y = \frac{1}{\sqrt{K}} \sinh L\sqrt{K}; S'_y = \frac{dS_y}{dL} = C_y \end{cases} \quad (13.35)$$

6605  $K > 0$  for a focusing quadrupole (by convention, in the  $(x, x')$  plane, thus defocusing  
 6606 in the  $(y, y')$  plane). Permute the horizontal and vertical  $2 \times 2$  sub-matrices in the  
 6607 case of a *defocusing* quadrupole.

### 6608 13.4.2.2 Electrostatic Quadrupole

6609 The hypotheses are those of Sect. 2.2.2: paraxial motion, field normal to velocity,  
6610 etc. Take the notations of Eqs. 2.25, 2.26 for the field and potential, electrodes in  
6611 the horizontal and vertical planes (Fig. 2.14). Electrode potential is  $\pm V/2$ , pole tip  
6612 radius  $a$ , so that  $K = -V/2a^2$  in Eq. 2.26. The equations of motion then write

$$\begin{cases} \frac{d^2x}{ds^2} + K_x x = 0 \\ \frac{d^2y}{ds^2} + K_y y = 0 \end{cases} \quad \text{with } K_x = -K_y = \frac{-qV}{a^2 m v^2} = \pm \frac{V}{a^2} \underbrace{\frac{1}{|E\rho|}}_{\text{electrical rigidity}} \quad (13.36)$$

6613 With that  $K = \frac{V}{a^2} \frac{1}{|E\rho|} = \frac{V}{a^2} \frac{1}{v(B\rho)}$  value ( $(B\rho) = p/q$  is the particle magnetic  
6614 rigidity), the transport matrix is the same as for the magnetic quadrupole, Eq. 13.35.

### 6615 13.4.3 Solenoid

6616 Assume a solenoid magnet with (OX) its longitudinal axis, and revolution symmetry,  
6617 With ( $O; X, r, \phi$ ) cylindrical frame, radius  $r$ , and angle  $\phi$  the coordinates in the X-  
6618 normal plane,  $B_\phi(X, r, \phi) \equiv 0$ . Take solenoid length  $L$ , mean coil radius  $r_0$  and an  
6619 asymptotic field  $B_0 = \mu_0 NI/L$  with  $NI =$  number of ampere-Turns,  $\mu_0 = 4\pi \times 10^{-7}$ .  
6620 The asymptotic field value is defined by

$$\int_{-\infty}^{\infty} B_X(X, r < r_0) dX = \mu_0 NI = B_0 L \quad \text{independent of } r \quad (13.37)$$

6621 There is a variety of methods to compute the field vector  $\mathbf{B}(X, r)$ . Opting for one  
6622 in particular may be a matter of compromise between computing speed and field  
6623 modeling accuracy. A simple model is the on-axis field

$$B_X(X, r = 0) = \frac{B_0}{2} \left[ \frac{L/2 - X}{\sqrt{(L/2 - X)^2 + r_0^2}} + \frac{L/2 + X}{\sqrt{(L/2 + X)^2 + r_0^2}} \right] \quad (13.38)$$

6624 with  $X = r = 0$  taken at the center of the solenoid. This model assumes that the coil  
6625 thickness is small compared to its mean radius  $r_0$ . The magnetic length comes out  
6626 to be

$$L_{\text{mag}} \equiv \frac{\int_{-\infty}^{\infty} B_X(X, r < r_0) dX}{B_X(X = r = 0)} = L \sqrt{1 + \frac{4r_0^2}{L^2}} > L \quad (13.39)$$

so satisfying

$$\text{on-axis } B_X(X = r = 0) = \frac{\mu_0 NI}{L \sqrt{1 + \frac{4r_0^2}{L^2}}} \xrightarrow{r_0 \ll XL} \frac{\mu_0 NI}{L}$$

6627 Maxwell's equations and Taylor expansions provide the off-axis field  $\mathbf{B}(X, r) =$   
 6628  $(B_X(X, r), B_r(X, r))$ . One has in particular in the  $r_0 \ll XL$  limit,

$$B_X(X, r) = \frac{\mu_0 NI}{L} \quad \text{and} \quad B_r(X, r) = \frac{-r}{2} \frac{dB_X}{dX} \quad (13.40)$$

6629 An other way to compute the field vector  $\mathbf{B}(X, r)$  is the elliptic integrals technique  
 6630 developed in [12], which constructs  $B_X(X, r)$  and  $B_r(X, r)$  from respectively

$$B_X(X, r) = \frac{\mu_0 NI}{4\pi} \frac{ck}{r} \mathcal{X} \left[ K + \frac{r_0 - r}{2r_0} (\Pi - K) \right] \quad (13.41)$$

$$B_r(X, r) = \mu_0 NI \frac{1}{k} \sqrt{\frac{r_0}{r}} [2(K - E) - k^2 K]$$

wherein  $K, E$  and  $\Pi$  are the three complete elliptic integrals,  $\mathcal{X}$  is an  $X$ - and  $L$ -dependent form factor, and

$$k = 2\sqrt{r_0 r} / \sqrt{(r_0 + r)^2 + X^2}; \quad c = 2\sqrt{r_0 r} / (r_0 + r)$$

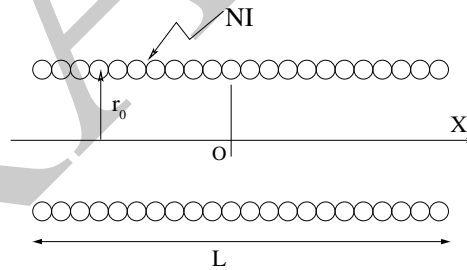


**Fig. 13.10** A sketch of a solenoid, and quantities used to define it

6631  
 6632 As an illustration, Fig. 13.11 displays a trajectory across a  $L = 1$  m solenoid  
 6633 and its fringe field extents, and the field experienced along that trajectory, in the  
 6634 axial model of Eq. 13.38. In the paraxial approximation, a pitch requires a distance  
 6635  $l = 2\pi/K$ , with  $K = B_0/B\rho$  the solenoid strength, which is a condition satisfied here  
 6636 if the fringe field extent is short enough ( $r_0$  is small enough).

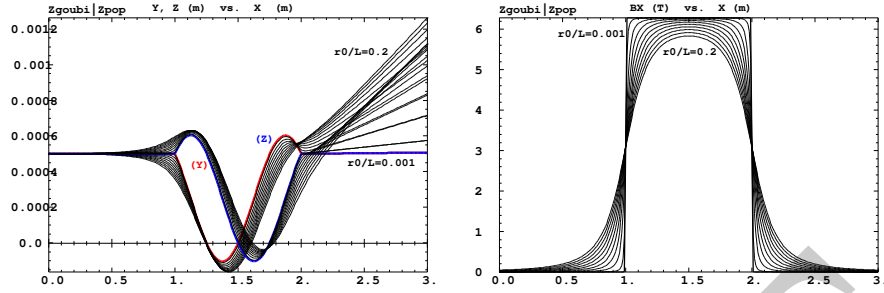


**Fig. 13.11** Left: Horizontal (Y) and vertical (Z) projections of a particle trajectory across a  $L = 1$  m solenoid, with additional 1 m extents upstream and downstream of the coil. The particle is launched with zero incidence, from transverse position  $Y = Z = 0.5$  mm. Sample solenoid radius/length values in the range  $0.001 \leq r_0/L \leq 0.2$  show that only for smallest  $r_0/L = 0.001$  does the trajectory end with  $Y = Z = 0.5$  mm and quasi-zero incidence (the thicker Y(X) and Z(X) curves), whereas greater  $r_0/L$  causes final Y(X) and Z(X) to be kicked away. Right: field  $B_X(X, r)$  experienced along the trajectory for the various  $r_0/L$  values, the steep fall-off case is for  $r_0/L = 0.001$ .

6637 *Linear approach*

6638 The equations of motion write, to the first order in the coordinates, in respectively  
6639 the central region (field  $B_s$ ) and at the ends (at  $s = s_{\text{EFB}}$ ),

$$\begin{cases} x'' - K z' = 0 \\ z'' + K x' = 0 \end{cases} \quad \text{and} \quad \begin{cases} x'' - \frac{K}{2} z \delta(s - s_{\text{EFB}}) = 0 \\ z'' + \frac{K}{2} x \delta(s - s_{\text{EFB}}) = 0 \end{cases} \quad (13.42)$$

6640 The first order transport matrix of a solenoid with length  $L$  writes

$$T_{\text{sol}} = \begin{pmatrix} C^2 & \frac{2}{K} SC & SC & \frac{2}{K} S^2 & 0 & 0 \\ -\frac{K}{2} SC & C^2 & -\frac{K}{2} S^2 & SC & 0 & 0 \\ -SC & -\frac{2}{K} S^2 & C^2 & \frac{2}{K} SC & 0 & 0 \\ \frac{K}{2} S^2 & -SC & -\frac{K}{2} SC & C^2 & 0 & 0 \\ 0 & 0 & 0 & 0 & 1 & \frac{L}{\gamma^2} \\ 0 & 0 & 0 & 0 & 0 & 1 \end{pmatrix} \quad \text{with} \quad \begin{cases} K = \frac{B_s}{B\rho} \\ C = \cos \frac{KL}{2} \\ S = \sin \frac{KL}{2} \end{cases} \quad (13.43)$$

6641 A solenoid rotates the decoupled axis longitudinally by an angle  $\alpha = KL/2 =$   
6642  $B_s L / 2B\rho$ .



## 6643 13.5 Data Treatment Keywords

### 6644 13.5.1 Concentration Ellipse: FAISCEAU, FIT[2], MCOBJET, ...

6645 It is often useful to associate the projection of a particle bunch in the horizontal,  
6646 vertical or longitudinal phase space with an *rms* phase space concentration ellipse  
6647 (CE). Various keywords in *zgoubi* resort to concentration ellipses:

- 6648 - FAISCEAU for instance prints out, in *zgoubi.res*, CE parameters drawn from  
6649 individual particle coordinates
- 6650 - random particle distributions by MCOBJET are defined using CE parameters.
- 6651 - ellipse parameters computed from CEs are possible constraints in FIT[2] pro-  
6652 cedures.

6653 Transverse phase space graphs by *zpop* also compute CEs.

6654 The CE method is resorted to in various exercises, for instance for comparison  
6655 of the ellipse parameters it gets from the *rms* matching of a bunch, with theoretical  
6656 beam parameters, as derived from first order transport formalism or computed from  
6657 rays by MATRIX, or TWISS.

6658 The method used in these various keywords and data treatment procedures is the  
6659 following. Let  $z_i(s)$ ,  $z'_i(s)$  be the phase space coordinates of  $i = 1, n$  particles in a set  
6660 observed at some azimuth  $s$  along a beam line or in a ring. The second moments of  
6661 the particle distribution are

$$\begin{aligned}\overline{z^2}(s) &= \frac{1}{n} \sum_{i=1}^n (z_i(s) - \overline{z}(s))^2 \\ \overline{zz'}(s) &= \frac{1}{n} \sum_{i=1}^n (z_i(s) - \overline{z}(s))(z'_i(s) - \overline{z'}(s)) \\ \overline{z'^2}(s) &= \frac{1}{n} \sum_{i=1}^n (z'_i(s) - \overline{z'}(s))^2\end{aligned}\quad (13.44)$$

6662 From these, a concentration ellipse (CE) is drawn, encompassing a surface  $S_z(s)$ ,  
6663 with equation

$$\gamma_c(s)z^2 + 2\alpha_c(s)zz' + \beta_c(s)z'^2 = S_z(s)/\pi \quad (13.45)$$

6664 Noting  $\Delta = \overline{z^2}(s)\overline{z'^2}(s) - \overline{zz'}^2(s)$ , the ellipse parameters write

$$\gamma_c(s) = \frac{\overline{z'^2}(s)}{\sqrt{\Delta}}, \quad \alpha_c(s) = -\frac{\overline{zz'}(s)}{\sqrt{\Delta}}, \quad \beta_c(s) = \frac{\overline{z^2}(s)}{\sqrt{\Delta}}, \quad S_z(s) = 4\pi\sqrt{\Delta} \quad (13.46)$$

6665 With these conventions, the *rms* values of the  $z$  and  $z'$  projected densities satisfy

$$\sigma_z = \sqrt{\beta_z \frac{S_z}{\pi}} \quad \text{and} \quad \sigma_{z'} = \sqrt{\gamma_z \frac{S_z}{\pi}} \quad (13.47)$$

### 6666 13.5.2 Transport Coefficients: MATRIX, OPTICS, TWISS, etc.

6667 Zgoubi does not know about matrix transport, it does not define optical elements  
 6668 by a transport matrix, it defines them by electrostatic and/or magnetic fields in  
 6669 space (and time possibly). Well, except for a couple of optical elements, for instance  
 6670 TRANSMAT, which pushes particle coordinates using a matrix, or SEPARA, an  
 6671 analytical mapping through a Wien filter. Zgoubi does not transport particles using  
 6672 matrix products either, it does that by numerical integration of Lorentz force equation.

6673 However it is often useful to dispose of a matrix representation of an optical  
 6674 element, of the transport matrix of a beam line, or the first or second order one-turn  
 6675 matrix of a ring accelerator. It may also be useful to compute the beam matrix and its  
 6676 transport. Several commands in zgoubi perform the necessary particle coordinates  
 6677 treatment to derive these informations. Examples are MATRIX: computation of  
 6678 matrix transport coefficients up to 3rd order, from initial and current coordinates of  
 6679 a particle sample. OPTICS transports a beam matrix, given its initial value using  
 6680 OBJECT[KOBJ=5.1] (see Sect. 13.5.2.2). TWISS derives a periodic beam matrix  
 6681 from a 1-turn mapping of a periodic sequence, and transports it from end to end so  
 6682 generating the optical functions along the sequence (Sects. 13.5.2.2, 13.5.2.3).

6683 These capabilities are used the exercises. It may be required for instance to  
 6684 compare transport coefficients derived from raytracing, with the matrix model of the  
 6685 optical element(s) concerned. Or to compute a periodic beam matrix in a periodic  
 6686 optical sequence, this is how betatron functions are produced, often for the mere  
 6687 purpose of comparisons with matrix code outcomes, or with expectations from  
 6688 analytical models.

#### 6689 13.5.2.1 Coordinate Transport

6690 In the Gauss approximation (*i.e.*, with  $\theta$  the angle of a trajectory to the reference  
 6691 axis,  $\sin \theta \sim \theta$ ), particles follow paths which can be described with simple functions:  
 6692 parabolic, sinusoidal or hyperbolic. A consequence is that a string of optical elements,  
 6693 and coordinate transport through the latter, can be handled with a simple mathematics  
 6694 toolbox. Taylor expansion (also known as transport) techniques are part of it, whereby  
 6695 a coordinate excursion  $v_{2i}$  (with index  $i = 1 \rightarrow 6$  standing for  $x, x', y, y', \delta s$  or  
 6696  $\delta p/p$ ) from some reference trajectory at a location  $s_2$  along the line is obtained from  
 6697 the excursions  $v_{1i}$  at an upstream location  $s_1$ , via

$$v_{2i} = \sum_{j=1}^6 R_{ij} v_{1j} + \sum_{j,k=1}^6 T_{ijk} v_{1j} v_{1k} + \sum_{j,k,l=1}^6 v_{1ijkl} v_{1j} v_{1k} v_{1l} + \dots \quad (13.48)$$

6698 This Taylor development can be written under matrix form, for instance to the  
 6699 first order in the coordinates, for non-coupled motion,

$$\begin{pmatrix} x \\ x' \\ y \\ y' \\ \delta s \\ \delta p/p \end{pmatrix}_2 = \begin{pmatrix} T_{11} & T_{12} & 0 & 0 & 0 & T_{16} \\ T_{21} & T_{22} & 0 & 0 & 0 & T_{26} \\ 0 & 0 & T_{33} & T_{34} & 0 & T_{36} \\ 0 & 0 & T_{43} & T_{44} & 0 & T_{46} \\ 0 & 0 & 0 & 0 & T_{55} & T_{56} \\ 0 & 0 & 0 & 0 & T_{65} & T_{66} \end{pmatrix} \begin{pmatrix} x \\ x' \\ y \\ y' \\ \delta s \\ \delta p/p \end{pmatrix}_1 = T(s_2 \leftarrow s_1) \begin{pmatrix} x \\ x' \\ y \\ y' \\ \delta s \\ \delta p/p \end{pmatrix}_1 \quad (13.49)$$

6700 These are the objects keywords as MATRIX [1, *cf.* Sect. 6.5] and OPTICS [1,  
6701 *cf.* Sect. 6.4] compute: the values of the transport coefficients, or transport matrices  
6702 to first and high order, are drawn from particle coordinates. Transport matrices of  
6703 common optical elements (drift, dipole, quadrupole, etc., magnetic or electrostatic),  
6704 are resorted to in the exercises for comparison with their matrix representation.

### 6705 13.5.2.2 Beam Matrix

6706 OPTICS and TWISS keywords cause the transport of a beam matrix. The former  
6707 requires an initial matrix: it is provided as part of the initial object definition, by  
6708 OBJET. The latter derives a periodic beam matrix from initial and final coordinates  
6709 resulting from raytracing throughout an optical sequence. Basic principles are re-  
6710 called here, This is the way it works in zgoubi, and in addition they are resorted to  
6711 in the exercises.

6712 In the linear approximation, the transverse phase space ellipse associated with a  
6713 particle distribution (for instance, the concentration ellipse, Sect. 13.5.1) is written  
6714 (with  $z$  standing for indifferently  $x$  or  $y$ )

$$\gamma_z(s)z^2 + 2\alpha_z(s)zz' + \beta_z(s)z'^2 = \frac{\varepsilon_z}{\pi} \quad (13.50)$$

6715 in which the ellipse parameters

$$\beta_z(s), \alpha_z(s) = -\frac{1}{2} \frac{d\beta_z}{ds}, \gamma_z(s) = \frac{1 + \alpha^2}{\beta_z} \quad (13.51)$$

6716 are functions of the azimuth  $s$  along the optical sequence. The surface  $\varepsilon_z$  of the ellipse  
6717 is an invariant if the beam travels in magnetic fields, however field non-linearities,  
6718 phase space dilution, etc. may distort the distribution and change the surface of its  
6719 *rms* matching concentration ellipse. In the presence of acceleration or deceleration  
6720 the invariant quantity is  $\beta\gamma\varepsilon_z$  instead, with  $\beta = v/c$  and  $\gamma$  the Lorentz relativistic  
6721 factor.

6722 The ellipse Eq. 13.50 can be written under the matrix form

$$\mathbf{1} = \tilde{T} \sigma_z^{-1} T \quad (13.52)$$

6723 with  $\sigma_z$  the beam matrix:

$$\sigma_z = \frac{\varepsilon_z}{\pi} \begin{pmatrix} \beta_z & -\alpha_z \\ -\alpha_z & \gamma_z \end{pmatrix} \quad (13.53)$$

6724 The ellipse parameters can be transported from  $s_1$  to  $s_2$  using

$$\sigma_{z,2} = T \sigma_{z,1} \tilde{T} \quad (13.54)$$

6725 with  $T = T(s_2 \leftarrow s_1)$  the transport matrix (Eq. 13.49) and  $\tilde{T}$  its transposed. This can  
6726 also be written under the form

$$\begin{pmatrix} \beta_z \\ \alpha_z \\ \gamma_z \end{pmatrix}_2 = \begin{pmatrix} T_{11}^2 & -2T_{11}T_{12} & T_{12}^2 \\ -T_{11}T_{21} & T_{21}T_{12} + T_{11}T_{22} & -T_{12}T_{22} \\ T_{21}^2 & -2T_{21}T_{22} & T_{22}^2 \end{pmatrix}_{s_2 \leftarrow s_1} \begin{pmatrix} \beta_z \\ \alpha_z \\ \gamma_z \end{pmatrix}_1 \quad (13.55)$$

6727 (subscripts 1, 2 normally hold for horizontal plane motion,  $z = x$ : change to 3, 4  
6728 for vertical motion,  $z = y$ ). This beam matrix formalism can be extended to the  
6729 longitudinal phase space and coordinates  $(\delta s, \delta p/p)$ , a  $6 \times 6$  beam matrix can be  
6730 defined,

$$\sigma = \begin{pmatrix} \sigma_{11} & \sigma_{12} & 0 & 0 & 0 & \sigma_{16} \\ \sigma_{21} & \sigma_{22} & 0 & 0 & 0 & \sigma_{26} \\ 0 & 0 & \sigma_{33} & \sigma_{34} & 0 & \sigma_{36} \\ 0 & 0 & \sigma_{43} & \sigma_{44} & 0 & \sigma_{46} \\ 0 & 0 & 0 & 0 & \sigma_{55} & \sigma_{56} \\ 0 & 0 & 0 & 0 & \sigma_{65} & \sigma_{66} \end{pmatrix} \quad (13.56)$$

6731 This can be generalized to non-zero anti-diagonal coupling terms, if motions are  
6732 coupled.

### 6733 13.5.2.3 Periodic Structures

6734 In the hypothesis of an  $S$ -periodic structure: a long beam line with repeating pattern,  
6735 a cyclic accelerator, transverse motion stability requires the transport matrix over a  
6736 period, from  $s$  to  $s + S$  to satisfy

$$[T_{ij}](s + S \leftarrow s) = I \cos \mu + J \sin \mu \quad (13.57)$$

6737 where  $\mu = \int_{(s)} ds/\beta$  is the betatron phase advance over the period (independent of  
6738 the origin),

$$I = \begin{pmatrix} 1 & 0 \\ 0 & 1 \end{pmatrix} \text{ is the identity matrix, } J = \begin{pmatrix} \alpha_z(s) & \beta_z(s) \\ -\gamma_z(s) & -\alpha_z(s) \end{pmatrix} \text{ (and } J^2 = -I) \quad (13.58)$$

## 6739 13.6 Exercises

### 6740 13.4 Magnetic Sector Dipole

6741 Solution: page 605.

6742 (a) Simulate a  $\rho = 1$  m radius,  $\alpha = 60$  degree sector dipole with  $n=-0.6$  field  
 6743 index, in both cases of hard edge and of soft fall-off fringe field model. Find the  
 6744 reference arc, such that  $\int_{\text{arc}} B ds = BL$  with  $L$  the arc length in the hard-edge model  
 6745 and  $B$  the field along that arc.

6746 Make sure the reference arc has the expected length.

6747 Produce the field along the reference arc, for a few different values of the fringe-  
 6748 field extent.

6749 (b) A possible check of the first order: `OBJET[KOBJ=5], MATRIX[IORD=1,IFOC=0]`  
 6750 can be used to compute the transport matrix from the rays. Compare what it gives  
 6751 with theory.

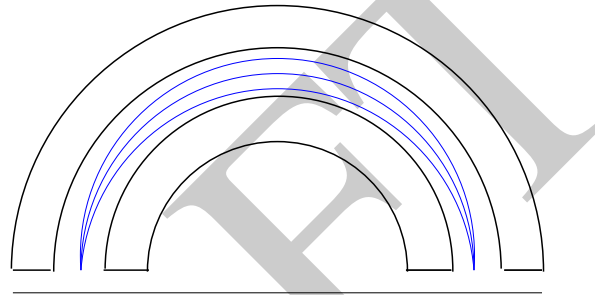


**Fig. 13.12** Focusing by a  
180 deg dipole

6752 (c) Consider a 180 deg wedge sector with uniform field. Show the well known  
 6753 geometrical property (cf. Sect. 3.2.2): this bend re-focuses at its exit EFB a diverging  
 6754 beam launched from the entrance EFB along the reference radius (Fig. 13.12).

6755 Test the convergence of the numerical solution versus integration step size.

6756 (d) Transport a proton along the reference axis, injected with its spin tangent to  
 6757 the axis. Compare spin rotation with theory.

6758 Test the convergence of the numerical solution versus integration step size.

### 6759 13.5 Solenoid

6760 Solution: page 609.

6761 An introduction to SOLENOID.

6762 (a) Reproduce Fig. 13.11. Use both fields models of Eqs. 13.38, 13.41 and compare  
 6763 their outcomes, including the first order paraxial transport matrices, higher order as  
 6764 well (computed from in and out trajectory coordinates).

6765 (b) Compare final coordinates in (a) with outcomes from the first order transport  
 6766 formalism (Sect. 13.4.3).

6767 (c) Make a 1-dimensional (on-axis) field map of a  $r_0 = 10$  cm,  $L = 1$  m solenoid  
 6768 (namely, a map  $B_{X,i}(X_i)$  of the field at the nodes of a X-mesh with mesh size  
 6769  $X_{i+1} - X_i$ ). Reproduce the trajectory in (a) (case  $r_0 = 10$  cm) using that field map,  
 6770 with the keyword BREVOL. Check the convergence of the final particle coordinates,  
 6771 using the field map, depending on the mesh size.

6772 **References**

- 6773 1. Méot, F.: Zgoubi Users' Guide.  
6774 <https://www.osti.gov/biblio/1062013-zgoubi-users-guide> Sourceforge latest version:  
6775 <https://sourceforge.net/p/zgoubi/code/HEAD/tree/trunk/guide/Zgoubi.pdf>  
6776 2. The AGS at the Brookhaven National Laboratory: <https://www.bnl.gov/rhic/AGS.asp>  
6777 3. The CERN PS: <https://home.cern/science/accelerators/proton-synchrotron>  
6778 4. Volk, James T.: Experiences with permanent magnets at the Fermilab recycler ring.  
6779 James T Volk 2011 JINST6 T08003. [https://iopscience.iop.org/article/10.1088/1748-](https://iopscience.iop.org/article/10.1088/1748-0221/6/08/T08003/pdf)  
6780 [0221/6/08/T08003/pdf](https://iopscience.iop.org/article/10.1088/1748-0221/6/08/T08003/pdf)  
6781 5. Dutheil, Y.: A model of the AGS based on stepwise ray-tracing through the measured field maps  
6782 of the main magnets. Proceedings of IPAC2012, New Orleans, Louisiana, USA, TUPPC101,  
6783 1395-1399.  
6784 <https://accelconf.web.cern.ch/IPAC2012/papers/tuppc101.pdf>  
6785 Méot, et al.: Modeling of the AGS using zgoubi - status. Proceedings of IPAC2012, New  
6786 Orleans, Louisiana, USA, MOPPC024, 181-183.  
6787 <https://accelconf.web.cern.ch/IPAC2012/papers/moppc024.pdf>  
6788 6. Enge, H. A.: Deflecting magnets. In: Focusing of Charged Particles, ed. A. Septier, Vol. II,  
6789 pp. 203-264, Academic Press Inc., 1967  
6790 7. Thern, R. E, Bleser, E.: The dipole fields of the AGS main magnets, BNL-104840-2014-  
6791 TECH, 1/26/1996.  
6792 <https://technotes.bnl.gov/PDF?publicationId=31175>  
6793 8. Méot, F., Ahrens L., Brown, K., et al.: A model of polarized-beam AGS in  
6794 the ray-tracing code Zgoubi. BNL-112453-2016-TECH, C-A/AP/566 (July 2016).  
6795 <https://technotes.bnl.gov/PDF?publicationId=40470>  
6796 9. Méot, F., Lemuët, F.: Developments in the ray-tracing code Zgoubi for 6-D multiturn tracking  
6797 in FFAG rings. NIM A 547 (2005) 638-651.  
6798 10. Leleux, G.: Accélérateurs Circulaires. Lectures at the Institut National des Sciences et Tech-  
6799 niques du Nucléaire, CEA Saclay (July 1978), unpublished  
6800 11. Credit: Brookhaven National Laboratory.  
6801 <https://www.flickr.com/photos/brookhavenlab/8495311598/in/album-72157611796003039/>  
6802 12. Garrett, M.W.: Calculation of fields [...] by elliptic integrals. In: J. Appl. Phys., 34, 9, Sept. 1963